Temperature dependence of transit currents in a one-dimensional polymer single crystal

1992 J. Phys.: Condens. Matter 4 6613

(http://iopscience.iop.org/0953-8984/4/31/013)

J. Phys.: Condens. Matter 4 (1992) 6613–6628. Printed in the UK

Temperature dependence of transit currents in a one-dimensional polymer single crystal

N E Fisher† and D J Willock‡

† Department of Physics, King's College London, Strand, London WC2R 2LS, UK
‡ Chemistry Department, University College London, Christopher Ingold Laboratories, 20 Gordon Street, London WC1H 0AJ, UK

Received 28 April 1992

Abstract. Time of flight experiments are performed over a range of temperatures (from 77 K up to 380 K) on the one-dimensional semiconductor single-crystal PDATS, using localized carrier generation on the (100) face. The transit profiles are found to become more dispersive at the reduced temperatures with their corresponding transit times becoming longer, and this we attribute to prolonged trap-release times from Coulomb traps. We fit these data to a trapping model in which the on-chain drift of the carriers is field saturated as proposed by Wilson but interspersed with frequent Coulomb trapping. We find that this model (to a first approximation) is physically reasonable at the temperatures used, provided the trend of trap-release probability with temperature (as well as field), as predicted by Blossey for one-dimensional carrier pair separation, is taken into account.

1. Introduction

PDATS (the polymer bis(p-toluene sulphonate) ester of 2,4-hexadiyne-1,6-diol) is easily produced as millimetre-sized single crystals in which the polymer backbone direction is well defined and common to all chains in the sample [1]. Because the chain separation is large (0.7 nm) compared to the repeat unit distance on a chain (0.45 nm) [2], each may be considered as an independent, quasi-one-dimensional semiconductor. Dark conductivity measurements along and perpendicular to the chains by Siddiqui and Wilson [3], show an anisotropy of over 1000 reflecting this one-dimensional nature. Experiments on PDATS may then offer an insight into one-dimensional carrier motion.

Before describing the temperature dependence work of the transit currents in this material, we shall briefly review the salient points of our earlier paper on the room temperature results [4].

The experimental arrangement for observing these transits is shown in figure 1; a sample of length D in the chain direction is overlaid with an opaque mask on the (100) face, containing a slit of width d. Following a laser pulse of duration 10 ns and photon energy 3.68 eV, carriers of both signs are generated within the slit, in a skin depth of 0.5 μm. Depending on the polarity of the applied voltage (V), one sign of carrier traverses an average distance of $L = D - d/2$ under the action of the applied field $F = V/D$ which is orientated along the chain direction, while the other sign discharges almost immediately at its nearest electrode.

0953-8984/92/316613+16$04.50

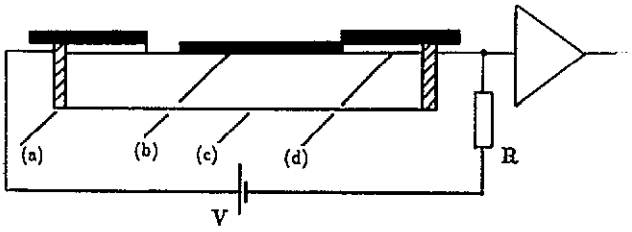

Figure 1. Experimental arrangement for transit current experiment on the (100) face in PDATS. (*a*) Silver-paste. (*b*) Opaque optical mask with slit width d. (*c*) PDATS crystal. (*d*) Evaporated Ag electrodes.

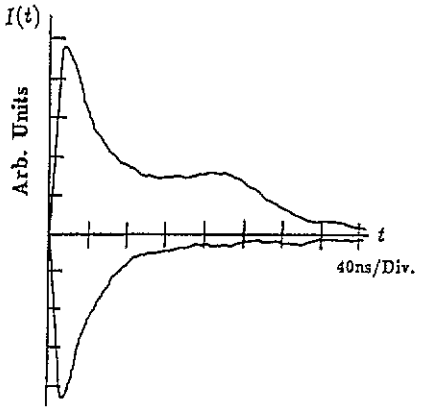

Figure 2. Current profiles for V negative (upper trace) and V positive (lower trace). Incident laser intensity is 1×10^5 W m^{-2} and F is 2.47×10^6 V m^{-1}.

Time of flight signals were observed for the electron transits while only featureless decays were observed for the hole 'transits', as in figure 2. It was concluded therefore, that the electrons are the dominant current carriers.

With reference to figure 2, the transit time t_τ of the faster carriers in traversing this distance L, was found by estimating the onset of the sharp decay at the shoulder. A drift velocity (v_d) and mobility (μ) was thus deduced using

$$v_d = L/t_\tau \tag{1}$$

$$\mu = v_d/F. \tag{2}$$

Using relation (1), a typical plot of the field dependence with drift velocity at room temperature is shown in figure 3 for a sample with $D = 300$ μm and using a slit of width of about 60 μm. Here, we noted that at low fields the drift velocity was approximately linear with field but at the higher fields, it tended to saturate at some acoustic velocity. In order to quantify this, we proposed a simple model in which the intrinsic on-chain motion of the carrier was that of the solitary wave acoustic polaron (SWAP) as proposed by Wilson [5] (which exhibits an intrinsic on-chain field independent acoustic velocity) but whose observed drift was dominated by shallow field dependent traps (or barriers). We envisaged a SWAP drifting along a chain at its intrinsic velocity v_0 until it encounters a trap into which it falls. After a time τ_b it is released, thereafter to continue its drift until it encounters the next trap. With the distance the carrier drifts taken as L, and with N traps present within L, its observed

transit time is

$$t_\tau = t_0 + N\tau_b \tag{3}$$

where $t_0 = L/v_0$ and $N\tau_b$ is the total delay time due to traps. In general, the probability per unit time of trap escape is

$$1/\tau_b = \langle t(a)\phi(a)\rangle \tag{4}$$

where $t(a)$ is the probability in unit time that a trapped carrier, ionizes and acquires thermal kinetic energies at a distance a from the trap and $\phi(a)$ is then the field dependent probability that the carrier avoids returning to the trap. For charged trap escape (and with the assumption that $t(a)$ is unaffected by field) Wilson [6] shows that

$$t(a) \propto \exp(-U_T/kT + U_a/kT) \tag{5}$$

$$\phi(a) \propto F\exp(-U_a/kT) \tag{6}$$

where U_T is the trap depth and U_a the potential energy of the carrier at a.

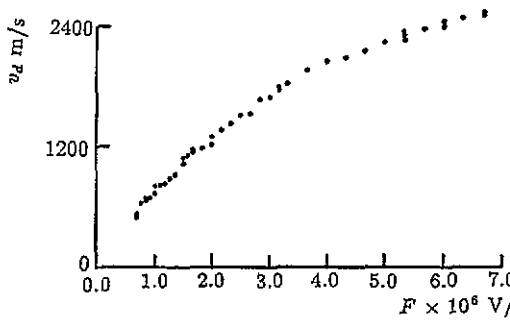

Figure 3. Field dependence of drift velocity for sample with D about 300 μm.

Thus the trap-release time is given by

$$\tau_b = (A/F)\exp(U_T/kT) \tag{7}$$

where A is a temperature and field independent constant. Hence

$$t_\tau = t_0 + (B/F)\exp(U_T/kT) \tag{8}$$

and

$$v_d = 1/[1/v_0 + (C/F)\exp(U_T/kT)] \tag{9}$$

where $B = NA$, v_d is the observed trap-limited drift velocity ($v_d = L/t_\tau$), $C = NA/L$ and N, in the context of experiment, is the number of traps of average depth U_T sampled by the faster carriers in traversing this distance L.

We then tested the validity of equation (9) by re-plotting the typical data of figure 3, as in figure 4. We noted a non-zero intercept on the ordinate axis which indicated to us a SWAP intrinsic velocity of between 3000 and 4000 $m\,s^{-1}$ (which we take as

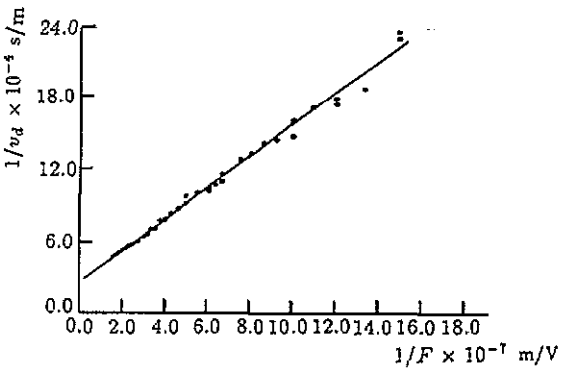

Figure 4. Plots of data from figure 3 following equation 9.

about 3600 m s^{-1} [7]). Thus, we proposed that at low fields the drift velocity is trap-limited with a trap-release time approximately inversely proportional to the applied field but as the field is increased, the observed trap-limited drift velocity asymptotically approaches the intrinsic SWAP velocity as trap-release times become shorter.

We conclude this section by stating that we observed trap-limited low field mobilities of the order 10^{-4} m^2(Vs)$^{-1}$ within sample lengths down to 50 μm, which is in broad agreement with the conclusions of Bassler *et al* [8,9], Heeger *et al* [10] and also another time of flight technique by one of the authors [11] but not in our opinion, reconcilable with the ultra-high low field mobilities and macroscopic inter-trap distances claimed by Donovan and Wilson [12,13].

2. Experimental arrangement and results

The sample/mask arrangement is again that shown in figure 1. Here, the sample is contacted to a quartz slide using heat sink compound. The slide is then contacted to the cold finger of a nitrogen cryostat, again using heat sink compound, in order to obtain good thermal contact. Before measuring a transit current, the cold finger is maintained at a given temperature for long times to ensure that the sample and the cold finger temperatures are the same.

The sample to be used has an inter-electrode separation (D) of about 400 μm and is held under a vacuum of 10^{-6} Torr. As with our previous experiments, this sample we denote as oxygen-free, meaning that the crystal was grown in an oxygen-free environment [14,15]. Again, a 10 ns, 3.68 eV laser pulse is used to generate the carriers in a slit of width, d, about 60 μm. The intensity of this laser pulse is kept low (about 3×10^8 W m^{-2}) for two reasons. Firstly, in order to minimize any possible space charge effects by the carriers themselves in disturbing the applied F field [7,16,17] and secondly, since the heat capacity of these crystals has been measured to be 0.978 J g^{-1} K^{-1} at 300 K varying down to 0.324 J g^{-1} K^{-1} at 80 K [18] any heating effects by the laser pulse will be small. (Here, we have made the approximation that all the incident radiation will be absorbed uniformly in the crystal's skin depth. Since the density of PDATS has been measured to be 1.48×10^6 g m^{-3} [19], this implies a temperature rise of only a fraction of a degree.)

Using this arrangement then, figure 5 and figure 6 each show the transit current profiles at three temperatures for a high field and a low field, respectively. We note that both the transit time lengthens (as estimated on each of the figures) and the profiles become more dispersive, as the temperature is reduced. In addition, the

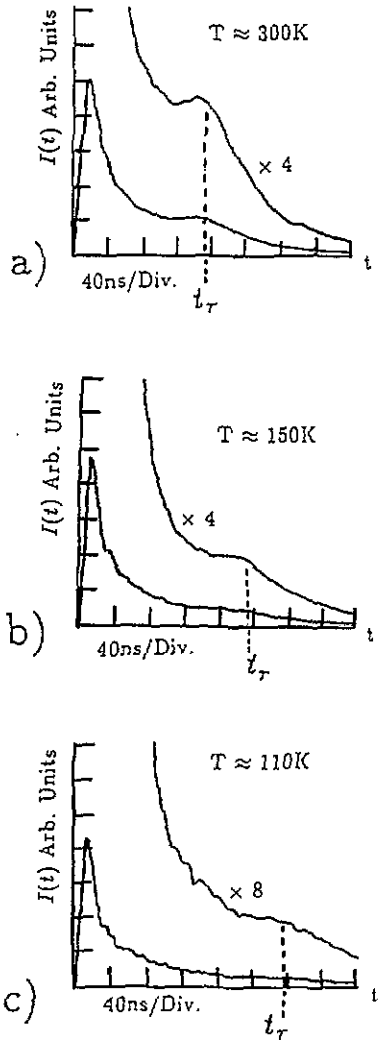

Figure 5. Temperature dependence of transit profiles at −1300 V. The $I(t)$ arbritary units of (b) and (c) are twice the sensitivity of (a) to show the gradual reduction of the photocurrents as the temperature is reduced. In each case the transition region is magnified by the amount shown.

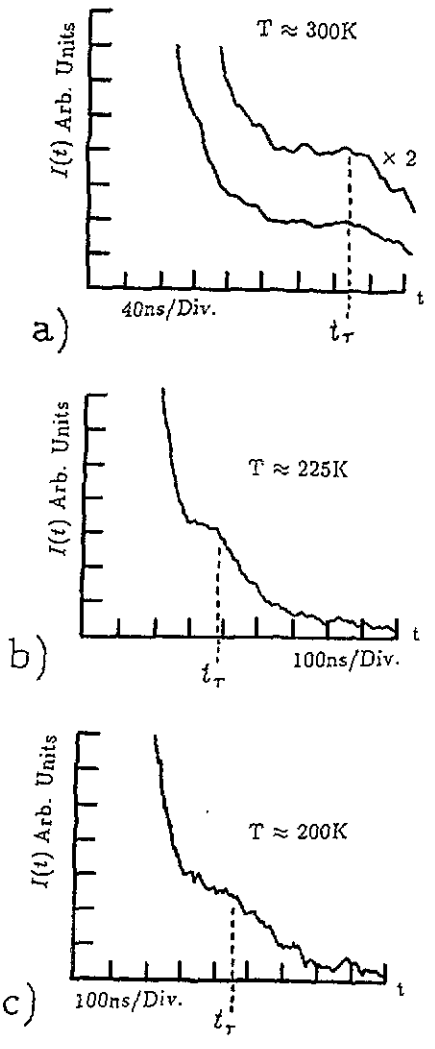

Figure 6. Temperature dependence of transit profiles at −400 V.

overall magnitude of the currents also reduces. Thus, we deduce that carrier transport is Coulomb trap-limited as opposed to barrier-limited since the latter mode would not be expected to exhibit this temperature dependence and that these characteristics as the temperature is reduced, are due to the trap-release times becoming sufficiently long so that carrier propagation becomes more dispersive. (Similar observations have been reported on for example, a-Se [20].) This dispersion can be dramatically seen in figure 7, which shows a comparison of an electron transit with its corresponding hole 'transit' at 77 K for the high field used in figure 5; at 300 K (of figure 5) a clearly defined time of flight signal is observed while at 77 K, this electron transit is almost

featureless.

We also performed these experiments at elevated temperatures up to 380 K and observed little change in the transit times (and magnitudes of currents) when compared to the room temperature results [7].

The next section attempts a quantitative analysis of carrier propagation at these low temperatures based on the model of section 1. As such, the data to be used has to exhibit a clearly defined time of flight signature from which a transit time may be estimated. However, because of the increased dispersion of the current profiles due to reduced temperature and/or field [4], our experimental range is limited. Nevertheless, we have obtained results using applied voltages from 400 V to 1300 V. (These results are all illustrated in reference [7].)

3. Analysis of results

To make the following analysis as objective as possible, the least-squares method is used to fit the data points from which gradients need to be found.

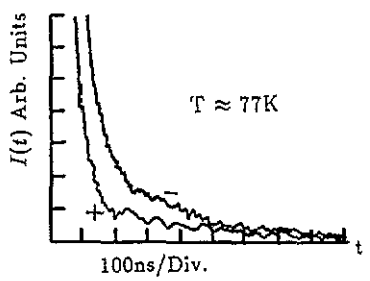

Figure 7. Current profiles for +1300 V (+) and for −1300 V (−).

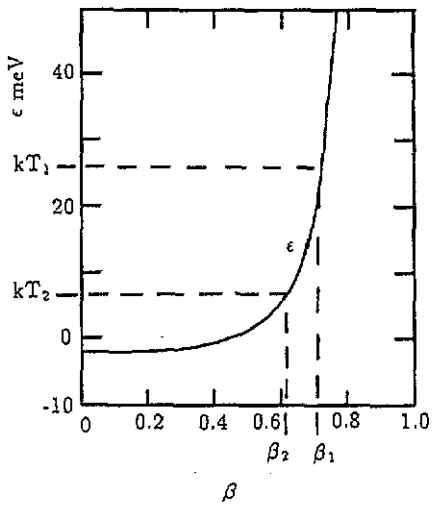

Figure 8. The total energy of the SWAP as a function of $v_0/v_s(=\beta)$ as calculated by Wilson [5]. The two values of kT are for thermal equilibrium energy at 300 K (1) and 77 K (2) with β_1 and β_2 their corresponding values.

Our model for carrier motion in PDATS summed up in equation (9) splits carrier motion into two distinct parts; intrinsic on-chain motion interspersed with frequent trapping events. We consider first the intrinsic on-chain drift of the SWAP. This we have taken to be independent of temperature and we justify this for two reasons. Firstly, we consider the derivation of the SWAP [5]: Wilson uses the total energy of the SWAP to define its saturated drift velocity as a fraction of the sound velocity, v_s. We show a plot of his calculations (taken from [5]) in figure 8; at room temperature the SWAP velocity saturates at $0.715v_s$ for a SWAP in thermal equilibrium

with its surroundings, while its corresponding value at 77 K is $0.61v_s$. This gives only a 15 per cent change in v_0 at these two temperatures. Because most of our analysis is at about 200 K and about 150 K, this means that the expected change of v_0 will be small. Secondly, as the temperature is reduced we consider that it is the increasingly extended temperature dependent trap-release times which dominate further the observed drift velocity over the intrinsic drift velocity. We conclude therefore, that any change in the intrinsic drift velocity, for most of the temperature range used here, is a relatively minor effect.

We start by noting that equation (8) suggests an Arrhenius plot; this we show in figure 9 for different applied fields. Here, we have taken v_0 to be 3600 $m\,s^{-1}$ which is a value deduced from our previous room temperature results and, as will be seen, appears to be a reasonable number for this particular sample. Inspection of figure 9 shows that the observed activation energy is field dependent which then implies, in our opinion, a field-assisted barrier lowering process for the trap-release times. As may be seen however, this is something not taken into account in the simple form of equation (8). Nevertheless, we reconcile this as follows; we still assume that the carrier escape attempt rate $t(a)$ (equation (5)) is independent of the applied field. However, once thermalized at a, a carrier then 'sees' a barrier U_a (equation (6)) and it is this barrier which we take to be prone to the field lowering. Probably the simplest model to describe this, is the Poole–Frenkel (PF) effect [21,22] which we illustrate in figure 10. Here, (in our case) the carrier at a now 'sees' a field lowered barrier U_a' given by:

$$U_a' = U_a - \beta F^{1/2} \tag{10}$$

where U_a is the zero-field barrier height and $\beta F^{1/2}$ is the PF barrier lowering term with

$$\beta = 2(e^3/4\pi\epsilon\epsilon_0)^{1/2}. \tag{11}$$

It thus follows that the U_a of equation (6) is now replaced (perhaps heuristically) by U_a' and so equation (8) becomes

$$t_r = t_0 + (B/F)\exp(\Delta E/kT) \tag{12}$$

where $\Delta E = U_T - \beta F^{1/2}$. Fits to the data of figure 9 give ΔE as about 15, 22, 27 and 32 meV for applied voltages of −1300, −800, −578, and −400 V, respectively.

From the definition of ΔE and the results of figure 9, we construct a PF plot as in figure 11 and from this, again using a straight line fit, we deduce both a value for U_T of 53 meV which is a plausible value for a shallow trap, and an experimental value for β of 2.2×10^{-5} $eV(V\,m^{-1})^{-1/2}$. Taking the dielectric constant of PDATS to be 6 [23], equation (11) gives an expected value for β of 3.1×10^{-5} $eV(V\,m^{-1})^{-1/2}$. This is in reasonable agreement with its experimentally deduced value.

So far the model looks encouraging. However, these low temperature results now suggest that the form of equation (9) should be modified to

$$v_d = 1/[1/v_0 + (D/F)\exp(-\beta F^{1/2}/kT)] \tag{13}$$

where $D = C\exp(U_T/kT)$, i.e. with the PF barrier lowering term now taken into account in the exponent. To test for this exponential field dependence, we plot the

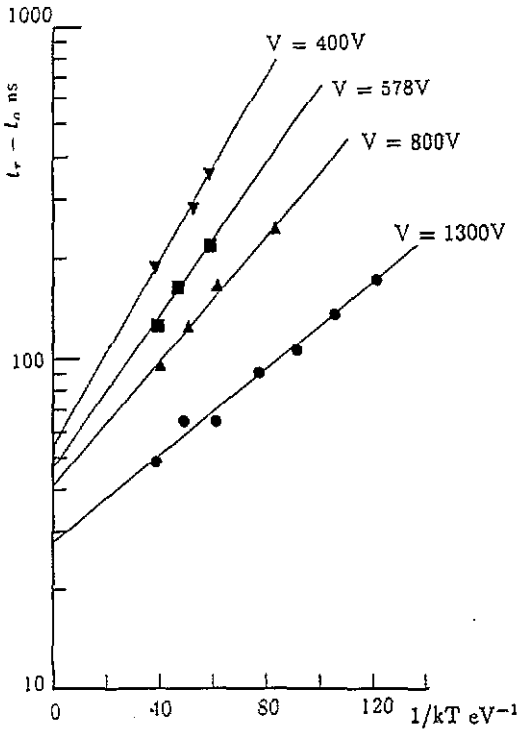

Figure 9. Activation plots using results from the experiments described in section 2.

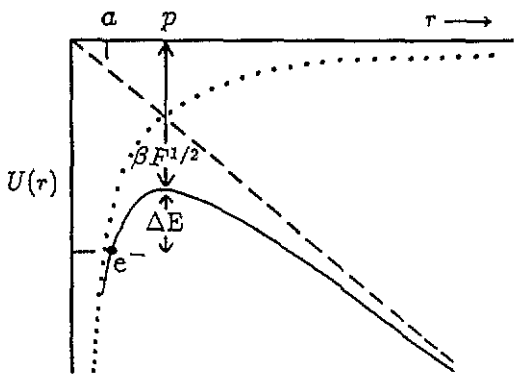

Figure 10. Illustration of Poole–Frenkel barrier lowering. The dotted line is the potential due to the Coulomb trap, the dashed line is the potential due to the applied field and the solid line is the sum of the two. a is the thermalization length of an electron and p is the position of the top of the barrier.

room temperature data of figure 3 as in figure 12. Here, the gradient of the data should give $-\beta/kT$, the expected value of which is represented by the dotted line in the figure. However as can be seen, the gradient indicated by the data is about zero and is a typical result found using other room temperature data [7]. If in addition, we now plot the data of figure 9 following equation (9) at three temperatures as in figure 13, the model following this equation (without the PF factor) breaks down at the two lower temperatures because extrapolation of the graphs to the ordinate axis implies that the intrinsic carrier velocity is increasing with decreasing temperature and indeed goes negative at the lowest temperature. (As expected, the room temperature data here gives an intrinsic drift velocity of about 3600 m s^{-1}.) These two graphs then,

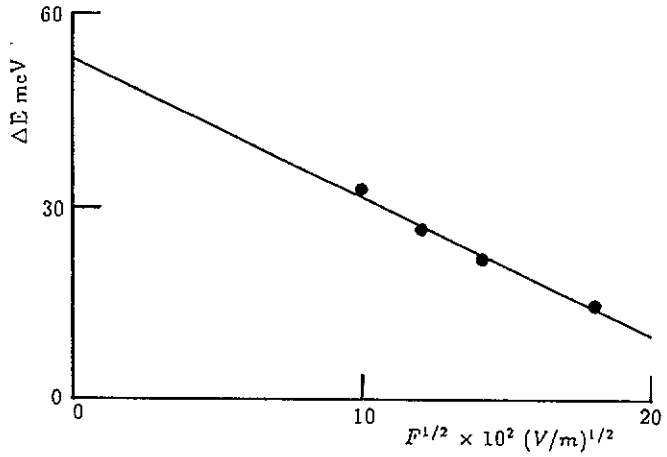

Figure 11. Poole–Frenkel plot using the ΔE values deduced from figure 9.

suggest to us the following: at room temperature there appears to be little or no barrier lowering and the data follows reasonably well equation (9). However, for the lower temperature data the model of this equation now breaks down. One possibility to explain this, is to consider whether in fact at these lower temperatures this barrier lowering effect does indeed need to be taken into account.

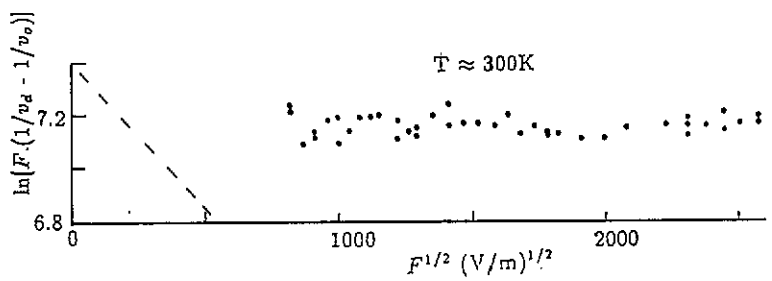

Figure 12. Data from figure 3 re-plotted following equation (13) to test for exponential field dependence. The gradient of the dashed line is the expected value of $-\beta/kT$ at 300 K.

To again test for this, we re-plot the data of figure 13 (as we did for the room temperature results in figure 12) as in figure 14 where once more, the gradients give $-\beta/kT$. We now find from fits to these data, that at 150 K $\beta_{150} = 1.7 \times 10^{-5}$ eV$(\mathrm{V\,m^{-1}})^{-1/2}$, at 200 K $\beta_{200} = 1.1 \times 10^{-5}$ eV$(\mathrm{V\,m^{-1}})^{-1/2}$, and at 300 K β_{300} is 0.5×10^{-5} eV$(\mathrm{V\,m^{-1}})^{-1/2}$ which we take to be about zero (bearing in mind the previous room temperature results). Substituting these experimental values of β into equation (13) for the two lower temperatures and then plotting the field dependence of drift velocity using the corresponding low temperature data in a form now following it, gives the plots of figure 15. As opposed to those of figure

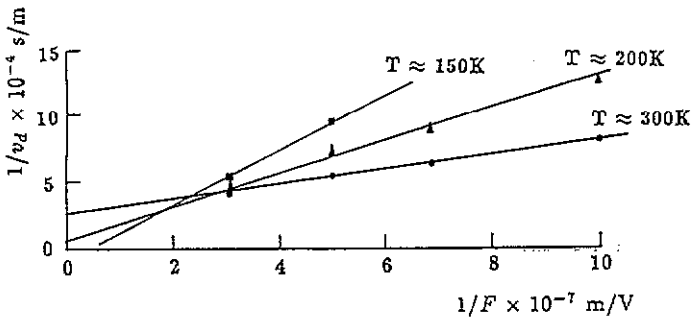

Figure 13. Plot of drift velocity data (used in figure 9) at various temperatures following equation (9).

13, the intrinsic drift velocity given by the ordinate axis intercept is now reasonable and in good agreement with the room temperature data. From this we propose that equation (9) reasonably describes the field dependence of the drift velocity at room temperature, but that this breaks down for the lower temperatures. Then equation (13) with its additional experimentally deduced PF term more aptly describes this field dependence. Also implicit in these results is the apparent dependence of the experimentally deduced values of β (an expected temperature independent quantity) with temperature; at high temperatures it is small or zero and at low temperatures it becomes larger possibly tending towards its expected value. This we now discuss.

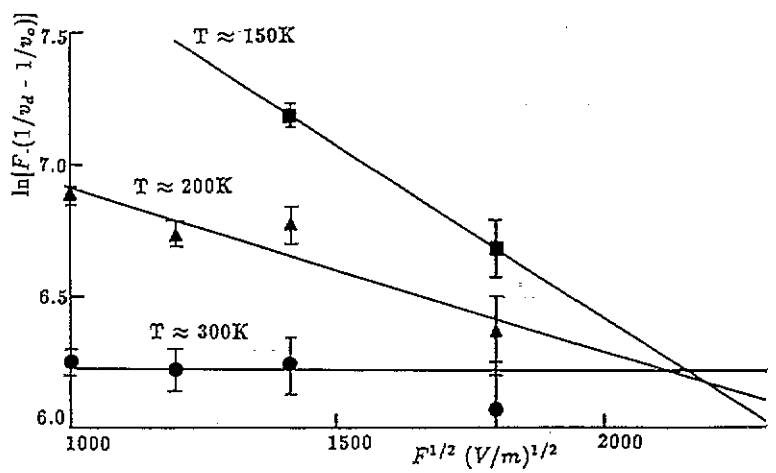

Figure 14. Data of figure 13 plotted following equation (13) to test for exponential field dependence.

4. Discussion

We recall that the equation for τ_b (equation (7)) was taken from reference [6]: this was based on the earlier calculations by Blossey [24] and Haberkorn and Michel-Beyerle (HMB) [25] who both considered the injection of charge carriers into insulators

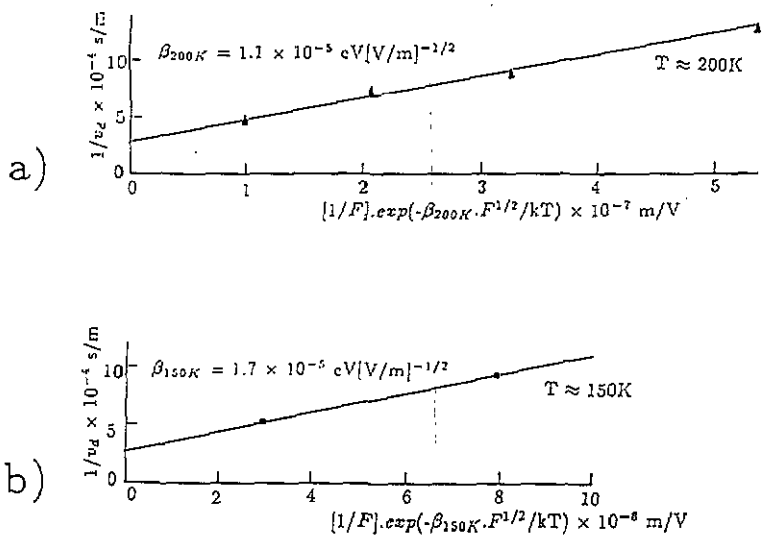

Figure 15. Re-plot of data from figure 13 following equation 13 using in each case the experimently determined values of β deduced from figure 14.

from metals. Their work gave a one-dimensional description of charge carrier pair separation under the influence of their mutual attraction and some externally applied field and has been found to be successful in describing (for example) the injection of electrons from Cu into CdS [26] and also carrier generation in PDATS e.g. [12] and [9] (though this has been questioned in the short time (ps) regime [10]).

Our problem of an electron moving away from a positively charged trap is in some ways similar to those addressed by Blossey etc. Here, they specifically deal with the escape probability $\phi(a)$ for an electron which has thermalized a distance a from its mirror charge (or hole). In our case, the trap may be modelled by a positive charge centre with the trapped electron already at a displacement b from the charge. This position (from the trap centre) is where the electron's electrostatic energy is the trap depth U_T. (We speculate on the physical nature of these traps in section 5.) From here, the carrier is excited and subsequently thermalizes at a larger displacement a from the positive charge (an event which has a probability in unit time $t(a)$ and which we still assume is field independent) after which its escape probability is then governed by $\phi(a)$.

The general equation for this quantity is given by HMB and Blossey:

$$\phi(a) = \int_0^a \exp(U(x)/kT)\,\mathrm{d}x \Big/ \int_0^\infty \exp(U(x)/kT)\,\mathrm{d}x \tag{14}$$

where $U(x)$ is the potential energy of the electron due to the combined field of (in our case) the positively charged trap and the applied field, and is given by:

$$U(x) = -e^2/4\pi\epsilon\epsilon_0 x - eFx. \tag{15}$$

Because the numerator of equation (14) is analytically intractable, Blossey calculates $\phi(a)$ numerically as a function of field in dimensionless units. Based on his

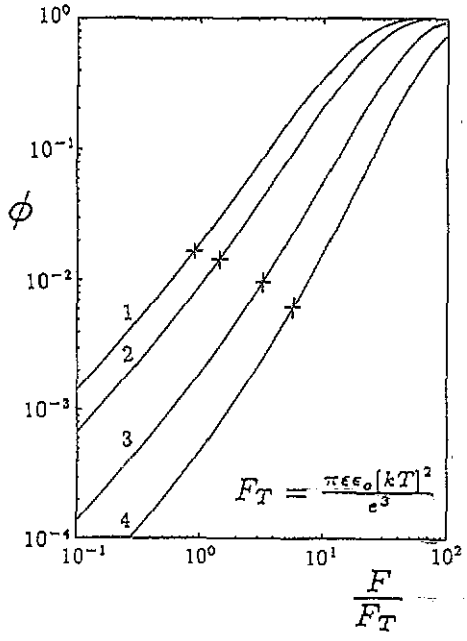

Figure 16. Thermalized electron escape probability as a function of field for temperatures of: (1) 380 K, (2) 300 K, (3) 200 K and (4) 150 K. Using a thermalization length a of 5 nm and a dielectric constant of 6 (for PDATS) these temperatures give values of a/X_T (the ratio used to generate plots following Blossey [24]) of: (1) 0.34, (2) 0.27, (3) 0.18 and (4) 0.14, where X_T is $e^2/(2\pi\epsilon\epsilon_0 kT)$. The plotted points correspond to an applied field of 1×10^6 V m^{-1}.

computations we generate our own plots as shown in figure 16. (Details of the routines used are given in [27].) We discuss why these particular curves were chosen and the points marked on them, shortly.

We now return to the question of why the experimental values of β in section 3 appear to tend towards zero (or possibly a very small value) as the temperature is increased. We consider first the asymptotic limits of $\phi(a)$ as deduced by Blossey. These are (at constant temperature):

$$\phi(a) \propto F \qquad \text{small } F, \text{ large } T \tag{16}$$

and,

$$\phi(a) \propto F^{3/4} \exp(\beta F^{1/2}/kT) \qquad \text{large } F, \text{ small } T. \tag{17}$$

and we note from this that at one limit $\phi(a)$ is linear with field while at the other it is superlinear because of the additional PF barrier lowering term found in the exponent. From figure 16 then, we can see that the degree of this barrier lowering is represented by the degree of the superlinearity of the curves, and that in the examples shown we are mostly at intermediate stages between these two limits.

What we propose is that a similar effect is occurring in our experiments. Namely at a given field, as the temperature is lowered the deduced experimental values of β tend towards the expected value as $\phi(a)$ approaches the small T limit. That is, in experiment for about the same fields, $\phi(a)$ moves over from the linear (or slightly superlinear) stage at room temperature towards the more strongly superlinear stage at low temperatures and that this change is reflected by an apparent increase in β which models this degree of superlinearity.

We can illustrate this idea as follows. Using Blossey's method, we generate plots for the field dependence of $\phi(a)$ specifically for PDATS (using $\epsilon = 6$) for a range of temperatures. On this diagram we can then plot a point on each curve for the same

applied field typical to that used in experiment in order to observe the degree of superlinearity at each temperature (for the same field).

In order to calculate these specific values of $\phi(a)$ it is necessary to know a and for that we must estimate U_a. Unfortunately, a direct determination of this quantity from our experiments is not possible since from equations (4), (5) and (6), U_a cancels.

However, we can attempt to make an upper bound estimate. We consider first the ionization probability $t(a)$ of equation (5) which in our case is given by the probability that a carrier in the trap aquires sufficient energy to escape the trap and then thermalizes at a. This is governed by the Boltzmann probability that a carrier moves between a state of energy U_T at b to the state of energy U_a at a. Since from experiment U_T has been estimated to be 53 meV, the minimum and most likely initial excess kinetic energy the electron will attain via a thermal process at ionization is about 53 meV. Here, we will take the trapped carrier to be a band electron, and consider scattering by acoustic phonons only since their coupling coefficient is known to be large in PDATS [28].

After a time t (following excitation) the thermalizing electron will have emitted t/τ phonons of average energy kT, where here τ is the mean scattering time for acoustic phonons.

Thus its kinetic energy at time t is given by:

$$E_{KE}(t) = U_T - (t/\tau)kT \tag{18}$$

where for the moment we have ignored the effect of the applied field and have assumed that phonon absorption is absent.

To obtain our upper bound estimate we assume that the electron always travels away from the trap centre. Therefore its velocity is always positive and given by:

$$v_e(t) = (2/m^*)^{1/2}(U_T - (t/\tau)kT)^{1/2} \tag{19}$$

where m^* is the effective mass of the electron.

In our simple model then, the electron has thermalized when its excess kinetic energy has reduced to zero i.e. in a time $(U_T/kT)\tau$. Thus by integrating equation (19)

$$a - b = (2/m^*)^{1/2}(2\tau/3kT)U_T^{3/2}. \tag{20}$$

Substituting values of $U_T = 53$ meV, $m^*/m = 0.25$ [29], $T = 300$ K, and $\tau = 0.6$ fs ([27] where the formalism of Conwell [30] is followed using the acoustic electron–phonon coupling coefficient as deduced by Kertesz *et al* [28] for PDATS), we obtain $a - b = 0.22$ nm.

It appears then, in this scenario, that electrons only move a short distance during thermalization and so U_a is approximately U_T. If phonon absorption and the effects of an applied field were to be included this estimate of $a - b$ may be increased. However, since our present value is so small compared to b we think it reasonable that U_a would still approximate to U_T. For example, in an applied field of 1×10^6 V m^{-1} (say) an electron travelling 0.22 nm gains only 0.22 meV which is negligible.

(It is interesting to note that in photo-absorption experiments using photon energies of up to 3.68 eV, the thermalization lengths of the generated electron-hole pairs were deduced to be about 10 nm [31,32]. Since the bandgap in PDATS is about

2.4 eV, we calculate from equation 20 a thermalization length of 27 nm for a photon energy of 3.68 eV and it is encouraging that this is a reasonable overestimate.)

Since we can estimate b from the relation

$$U_T = e^2/4\pi\epsilon\epsilon_0 b \tag{21}$$

it follows that a is approximately 5 nm. Using this value, figure 16 shows Blossey's expected curves for PDATS at temperatures of 380, 300, 200 and 150 K.

Marked on each is the point at which the field is 1×10^6 V m^{-1}. By comparing the regions at these points, it may be seen that the slope becomes more superlinear with decreasing temperature. We can quantify this by numerically calculating the gradient at these points. For 380 K this gives 1.20, for 300 K this gives 1.28, for 200 K this gives 1.48, and for 150 K this gives 1.67; a significant trend. Based on this example then, we would expect the low temperature experimental data to be more prone to barrier lowering than data taken at higher temperatures for about the same fields.

Qualitatively this can be understood by considering the following: An electron will diffuse easily to a distance r_{kT} away from a positively charged trap where r_{kT} is the Coulomb radius and is the trap/electron separation at which their Coulomb energy is equal to the electron's thermal energy. That is,

$$r_{kT} = e^2/4\pi\epsilon\epsilon_0 kT. \tag{22}$$

Depending on the relative position of r_{kT} with respect to the position of the top of the barrier p (see figure 10) which is given by,

$$p = (e/4\pi\epsilon\epsilon_0 F)^{1/2} \tag{23}$$

the potential experienced by the electron at r_{kT} is influenced to different degrees by the applied field. This can be seen from figure 10; if r_{kT} is much less than p (i.e. at high temperatures) then the potential experienced by the electron as it diffuses to r_{kT} is not significantly altered from the zero field case. On the other hand for r_{kT} closer to p (i.e. at lower temperatures), the potential experienced by it is more strongly affected by the applied field which then results in the observed barrier lowering.

It is also interesting to note from figure 16, that the change in $\phi(a)$ between 300 K and 380 K at 1.0×10^6 V m^{-1} is comparatively small and this may account for the observed negligible difference between the transit times obtained at these two temperatures mentioned in section 2.

In summary then, we take into account the PF approach to barrier lowering which itself is only an approximation to the more complete theory of Blossey and others. In our case equation (13) which incorporates the PF term, provides a more physically reasonable description of trap-limited electron transport in PDATS based on our trapping model, provided the experimentally deduced values of β are used. That is, a small or zero value at room temperature which tends towards its expected value at low temperatures. This is equivalent to tailoring the field superlinearity of trap-release to the temperature of the experiment.

Finally, it should be noted that this change in $\phi(a)$ with temperature has implications for our earlier treatment of the data. In figure 9 we showed activation plots for different fields to each of which we fitted a line. From this we deduced field dependent activation energies for use in the PF plot of figure 11. However, having now

taken into account the fact that the field dependence of $\phi(a)$ is itself temperature dependent, the data in the activation plots would now be expected to have a gradual non-linear dependence with $1/T$. Nevertheless, we consider it plausible that our straight line fits still give values for U_T but averaged over the temperature ranges used. Hence, U_T and β deduced from figure 11, and a, though reasonable, are only approximate values.

There is however, one encouraging aspect to this: to test for the sensitivity of U_T and hence a with the gradient $-\beta$ in the PF plot of figure 11, we plotted lines through each of the 4 experimental data points but now using the the theoretical value of $-\beta$ as their gradients. We found that their intecepts on the ordinate axis gave values of U_T varying from 63.3 to 70.8 meV which then corresponds to a spread in a from 3.4 to 3.8 nm with its average value being about 3.7 nm. It is encouraging then, that if we had used this value we would have 'rounded' this up to 4 nm which is very close to our initial estimate of 5 nm.

5. Conclusions

As far as we are aware, these results are the first reported temperature dependent transit current measurements on PDATS. We find currents that exhibit longer transit times and more dispersive profiles as the temperature is reduced and attribute this to prolonged trap-release times from Coulomb traps. Other workers e.g. [31,33] (and ourselves [27]) using uniform illumination techniques (that is using the experimental set-up of figure 1 but without the optical mask present) find the tail decay following a fast laser pulse narrows with temperature and like us attribute this to prolonged trap-release times.

We also find that our low temperature data fits (to a first approximation) our trapping model and gives reasonable values for the intrinsic on-chain drift of the SWAP provided the superlinear field dependence of $\phi(a)$ is taken into account—a trend predicted by Blossey's analysis.

The true nature of the trapping centres we observe in PDATS is difficult to discern from the work presented here. We can however suggest possible improvements which may reflect better the physical nature of the trap.

Because we base our model on Blossey, we assume that the trap is due to a full positive charge on a chain and at some separation from the trapped electron. However, because we are in a one dimensional system, we would in fact expect this charge to act as an infinite sink as the electron initially approaches it with resulting negligible probability of trap-release. Such a situation would then lead to observed monomolecular recombination. However, our earlier experiments show this recombination not to occur for these oxygen-free samples [15]. Hence, we speculate that the charge responsible for the trap is not on the chain (so allowing the electron a larger probability of trap-escape) but near enough so that Blossey's analysis still holds. Impurities are known to exist in PDATS [34,35] and our earlier experiments suggest that oxygen contamination may play a large part in their concentration [15].

Finally, we note that from our earlier paper on transit currents [4], we observed that as D was made smaller, so the transit currents obtained exhibited less dispersive profiles for the same applied fields. We would expect then, that if these experiments were to be repeated using much smaller inter-electrode distances it should be possible to obtain clearly defined time of flight signals over a greater range of temperatures

and fields than that used here. Such an increase in the amount of data would then support (or otherwise) our own observations and interpretations.

Acknowledgments

We thank Professor D N Batchelder (Leeds University) and Professor G Parish (University College London) for their useful comments. We are also grateful to Dr B J E Smith for supplying us with some excellent quality PDATS crystals. The experiments presented here were conducted at Queen Mary and Westfield College, London. This work has been supported by SERC (UK).

References

[1] Wegner G 1969 *Z. Naturf.* b **24** 824
[2] Pope M and Swenberg C E 1982 *Electronic Processes in Organic Crystals (Monographs on Physics and Chemistry of Materials No 39)* (Oxford: Oxford Science Publications)
[3] Siddiqui A S and Wilson E G 1979 *J. Phys. C: Solid State Phys.* **12** 4237
[4] Fisher N E and Willock D J 1992 *J. Phys.: Condens. Matter* **4** 2517
[5] Wilson E G 1983 *J. Phys. C: Solid State Phys.* **16** 6739
[6] Wilson E G 1979 *J. Phys. C: Solid State Phys.* **13** 2885
[7] Fisher N E 1990 *PhD Thesis* University of London
[8] Reimer B and Bassler H 1978 *Phys. Status Solidi* b **85** 145
[9] Blum T and Bassler H 1988 *J. Chem. Phys.* **123** 431
[10] Moses D and Heeger A J 1989 *J. Phys.: Condens. Matter* **1** 7395
[11] Fisher N E 1992 *J. Phys.: Condens. Matter* **4** 2543
[12] Donovan K J and Wilson E G 1981 *Phil. Mag.* B **44** 9
[13] Donovan K J and Wilson E G 1985 *J. Phys. C: Solid State Phys.* **18** L51
[14] Poole N J, Smith B J, Batchelder D N and Read R J 1986 *J. Mater. Sci.* **21** 507
[15] Fisher N E and Willock D J 1992 *J. Phys.: Condens. Matter* **4** 2533
[16] Many A, Weisz S Z and Simhony M 1962 *Phys. Rev.* **126** 1989
[17] Many A and Rakavy G 1962 *Phys. Rev.* **126** 1980
[18] Engeln I and Meissner M 1980 *J. Polym. Sci. (Phys.)* **18** 2227
[19] Kobelt D and Paulus E F 1974 *Acta Crystallogr.* B **30** 232
[20] Pfister G and Scher H 1978 *Adv. Phys.* **27** P747
[21] Poole H H 1916 *Phil. Mag.* **32** 112
[22] Frenkel J 1938 *Phys. Rev.* **54** 647
[23] Nowak R, Sworakowski J, Kutchta B, Bertault M, Schott M, Jakubas R and Kolodziej H A 1986 *Chem. Phys.* **104** 467
[24] Blossey F D 1974 *Phys. Rev.* B **9** 5183
[25] Haberkorn R and Michel-Beyerle M E 1973 *Chem. Phys. Lett.* **23** 128
[26] Mort J, Schmidlin F W and Lakatos A I 1971 *J. Appl. Phys.* **42** 5761
[27] Willock D J 1991 *PhD Thesis* University of London
[28] Kertesz M, Koller J and Azman A 1978 *Chem. Phys.* **27** 273
[29] Wilson E G 1975 *J. Phys. C: Solid State Phys.* **8** 727; 1980 *J. Phys. C: Solid State Phys.* **13** 2885
[30] Conwell E M 1980 *Phys. Rev.* B 1980 **22** 1761
[31] Donovan K J and Wilson E G 1986 *J. Phys. C: Solid State Phys.* **19** L357
[32] Lochner K, Reimer B and Bassler H 1976 *Phys. Status Solidi* b **76** 533
[33] Moses D, Sinclair M and Heeger A J 1987 *Phys. Rev. Lett.* **58** 2710
[34] Bloor D and Preston F H 1976 *Phys. Status Solidi* a **37** 427
[35] Siddiqui A S 1980 *J. Phys. C: Solid State Phys.* **13** 2147